Seismic Response Evaluation of Reinforced High Strength Concrete Columns based on the Modified Constitutive Model

Farzin Vahid-Vahdattalab[1], Javad Mokari Rahmdel[2], Erfan Shafei[3*]

[1] Master of Science, Structural Engineering, Urmia University of Technology

[2,3] Assistant Professor, Civil Engineering Faculty, Urmia University of Technology

* Corresponding Author: Tel: +98-44-3372-8180, E-mail: e.shafei@uut.ac.ir

Abstract

Current study deals with strength and seismic ductility assessment of reinforced high strength concrete (HSC) columns. We have studied the nonlinear response of HSC columns with various reinforcement and axial force ratios subjected to cyclic loading. Study consists of primary verification of mathematical nonlinear model and further calibration to ensure accuracy. An existing experimental work is assumed as verification pilot that consists of four columns. Column members differ in the strength and axial force. Concrete has 63.1 MPa mean strength and 0.3% crushing strain. The longitudinal and transverse reinforcements are according to ACI 318 regulations in experiment. We used the nonlinear fiber-element code in OpenSees environment for modeling and analysis of models. The existing proposed stress-strain curve is modified to ensure validity of assessment. Calibration procedure led to conclusion that the post-yield slope needs to be modified in HSC model as the average value of ACI 363 reference. We have developed twelve extra models to estimate the interaction of concrete strength, rebar ratio and the axial force effect on the seismic performance. Parametric study of calibrated models reveals that the seismic energy dissipation in HSC members is function of the provided longitudinal reinforcement ratio and lateral confining stirrup amount.

Keywords: *High Strength Concrete, Seismic Assessment, Modified Strength Model, Cyclic Loading, Second Order Force Effect, Reinforcement Ratio*

1. Introduction

Primarily, it is essential to have a short definition of HSC according to valid regulations. ACI Committee 363 [1] defined HSC as a concrete material with crushing strength (f'_c) higher than 41 MPa. HSC is used in high-rise and special structures such as dams and hydropower sub-structures. Various research works is conducted in the field of HSC and its feasible potential use in civil structural systems. Sugano et al. [2] have conducted effective research on the experimental seismic behavior of HSC columns, which are laterally reinforced with high strength steel bars. They revealed that the use of high or ultra-high strength steel bars is quite effective in confining HSC with strength increase up to 80 MPa. Therefore, they suggested the use of high or ultrahigh strength lateral reinforcements for the HSC columns subjected to axial compression. Xiao et al. [3] have conducted a broad research on the seismic performance evaluation of HSC columns with focus on shear strengths. Results revealed that the shear strength of the HSC columns withe shear failure mode was overestimated by the ACI 426 [4] relation, but the ACI 318 [5] relation estimated the shear strength with 10% deviation.

Ashour [6] has conducted a research on the effect of compressive strength and tensile reinforcement ratio on flexural behavior of HSC beams. Study revealed that for the same longitudinal reinforcement, the cracking moment increases as concrete compressive strength increases. In addition, the increase in concrete compressive strength leads to an increase in the flexural rigidity of reinforced concrete beam. Bing et al. [7] has conducted a research on the stress-strain curve of HSC confined by ultrahigh and normal-strength transverse reinforcements. Study revealed that the compressive strength of concrete determines the column ductility, particularly for strengths higher than 60 MPa. Regardless of the concrete compressive strength, a rise in the confinement ratio results in peak stress growth. In addition, results revealed that the enhancement in the ultimate strain of lateral confining system results in a decrease in the slope of softening branch of stress-strain curve. Kabir and Shafei [8] conducted studies on the lateral confining of HSC using FRP jackets subjected to eccentric axial loading in advance. The acquired results revealed that FRP confinement is also effective in strength and ductility enhancements of high strength columns. However, strengthening is much effective in normal strength concrete (NSC) than HSC since concrete does not exhibit adequate volumetric dilation to activate the FRP confinement.

Woods et al. [9] has conducted research about bending ductility of the rectangular HSC columns. Study revealed that there is an interaction between the ductility and the transverse reinforcement spacing. They noted that for a given tie spacing, there is a range of transverse reinforcement ratio which enhance the column ductility. Ho et al. [10] has conducted a research on the affectivity of adding additional confining system on the ductility improvement of HSC columns. Study presented that the stress-strain path of the concrete in confined columns are sensitive to the provided confining system. In addition, the design parameters of the confined concrete are determined by confinement characteristics, which are necessary for initial proportioning of HSC members. Results revealed that both the balanced reinforcement ratio and ultimate axial force capacity increase when the confining pressure is increased which finally improved the flexural ductility of the confined column. Hui et al. [11] has conducted research about empirical stress-strain models for unconfined HSC under uniaxial compression. Results approved that the empirical proposed model can efficiently cover the existing experimental data for normal weight HSC materials and can represent the mean stress-strain curve.

Ozbakkaloglu [12] has conducted research on the behavior of square and rectangular ultrahigh strength concrete-filled FRP tube (UHSCFFT) columns under axial compression. Study revealed that sufficiently confined square and rectangular columns could exhibit a compressive behavior with high ductility. However, the behavior of members is highly sensitive to the confining tube thickness. In other words, the tubes with thin walls do not provide sufficient confining pressure in order to allow columns to maintain their load carrying capacity beyond the peak load. In addition, the crushing strength of HSC materials with high strengths are more sensitive to the confining pressure than low strength ones. Kottb et al. [13] has conducted research on the behavior of HSC columns under eccentric axial loads. Study revealed that using normal longitudinal steel bar diameter in HSC columns is not adequate and leads to a catastrophic collapse. They have conducted analytical studies using existing semi-empirical material models of HSC with total assessment error of 17%, which approves additional studies for calibration of mathematical models for HSC material behavior.

2. Research Significance

The main criteria in the seismic application feasibility of HSC construction is the stability and ductility levels during quake excitations. On the other hand, the design regulations necessitate the designer provide a unified material response

curves for calculations and requirement controls. Thus, there is an essential need to provide the preliminary material constitutive curve for seismic excitation beside the static loads. HSC columns are the primary members that resist the quake-imposed energy during seismic action in moment frame systems, and therefore they need to be designed in dimension and material to do so. There is a serious lack in determination of initial design dimensions because there is not a unified regulation for the HSC materials. Seismic performance evaluation of such members depends directly on calibrated definition of stress-strain curve concerning the cyclic load protocols.

The HSC column ductility and its interaction with demand seismic performance is not specified in recent research works and therefore the goal of current study is to evaluate the existing material models and modify them, if required in order to satisfy the design prerequisite performance levels. Primary target of study is to assess the HSC compressive strength effect on the hysteretic load-deflection response and the dissipated energy under defined displacement protocols. Four square RC columns with HSC material, which is tested, by Xiao and Yun [14] is the basis of numerical simulation and should be calibrated according to presented experimental data. Extended study on present research work is to evaluate the accuracy and validity of the existing stress-strain curves for HSC which also considers the successive cracking and crushing of concrete.

3. Response Characterization

3.1 Experimental Background

Columns accepted as the pilot experimental database are in full-scale size and have square 510 mm cross section with a total height of 2032 mm as tested by Xiao and Yun Lateral loading point is elevated at 1778 mm height top of the footing. All columns are reinforced with four No. 36 (d=35.8 mm) bars plus four No. 29 (d=28.7 mm) bars, which provides a flexural reinforcement ratio of 2.6% [14]. The main testing parameters selected as parametric study were the transverse reinforcement ratio and the axial load ratio. The additional fly ash, silica fume, super-plasticizer and low water-to-cement ratio provide the design compressive strength from 34.5 MPa up to 64.1 MPa for HSC. Grade 420 (f_y=469 MPa) steel rebar are used as longitudinal reinforcement for all members beside both grade 420 and 520 (f_y=524 MPa) stirrups as transverse reinforcement of each three-column groups. The configuration of HSC-RC columns tested by Xiao and Yun is as demonstrated in **Figure 1**. The details of test members are as in **Table 1** reported by the researches.

The base of all columns were anchored to rigid base using post tensioning system which is assumed as full restrain in numerical model. In experimental procedure, due to restriction of axial load application, the value of vertical gravity load was changing as column was laterally displaced. However, this phenomenon is modeled exactly as occurring in real nature of structural columns since vertical load does not have any direction change in small drifts (lower than 6%). Therefore, the second order effect of axial load (P-Δ) is expressed in an acceptable way in simulation of current study than as applied in the experiments. The experiment uses external apparatus to apply the combined axial and vertical loading where the direction change of vertical load has not neglected in the test. This case lowers the effect of second order load effect in the test. However, we keep the direction of vertical load as constant and perpendicular to the foundation during the whole analysis, which is realistic in structural problems. This case shown as **Figure 2**. The axial load is constant over the period of testing although the lateral displacement has cyclic regime with increasing amplitudes. The time history of applied lateral relative displacement (Δ/L), drift, is according to **Figure 3** which

consists of six successive cycles with 0.5% drift increase at first followed by 1% three drift cycles up to rupture of member.

3.2 Material Mathematical Model

The basic stress-strain constitutive curve assumed for HSC is the model proposed by Bing et al. [7], which consists of three, continues relation as following. Assumed model is based on the Mander et al. [15] classic uniaxial curve for concrete compression. Model has quasi-linear pattern up to unconfined strength limit (f'_{co}) as **Equation 1** which is 64.1 and 62.1 MPa for HSC columns tested by Xiao and Yun. High strength nature of concrete leads to insensible transition between unconfined crushing strain (ε_{co}) and stirrup-confined crushing strain (ε_{cc}) as is expressed in **Equation 2**. Finally, the strength-degrading branch of the curve is defined as **Equation 3** with a linear descending up to $0.4f'_{cc}$ strength.

$$0 \le \varepsilon_c \le \varepsilon_{co} \rightarrow f_c = E_c\varepsilon_c + \frac{\left(f'_{co} - E_c\varepsilon_{co}\right)}{\varepsilon_{co}^{\,2}}\varepsilon_c^{\,2} \tag{1}$$

$$\varepsilon_{co} \le \varepsilon_c \le \varepsilon_{cc} \rightarrow f_c = f'_{cc} - \frac{\left(f'_{cc} - f'_{co}\right)}{\left(\varepsilon_{cc} - \varepsilon_{co}\right)^2} \times \left(\varepsilon_c - \varepsilon_{cc}\right)^2 \tag{2}$$

$$\varepsilon_c > \varepsilon_{cc} \rightarrow f_c = f'_{cc} - \beta\frac{f'_{cc}}{\varepsilon_{cc}} \times \left(\varepsilon_c - \varepsilon_{cc}\right) \ge 0.4f'_{cc} \tag{3}$$

$$f'_{cc} = f'_{co}\left[-0.413 + 1.413\sqrt{1 + 11.4\frac{f'_l}{f'_{co}}} - 2\frac{f'_l}{f'_{co}}\right] \tag{4}$$

Confined concrete strength (f'_{cc}) depends on the ratio of confining pressure (f'_l) to unconfined crushing strength (f'_{co}) as **Equation 4**. Parameters needed for above equations are elastic modules (E_c) as **Equation 5** proposed by ACI committee 363 [1] and softening slope (β). One of the necessary stages in curve definition is appropriate selection of β value. Relations proposing practical values for β are according to **Equation 6** up to **Equation 8** sets.

$$E_c = 3320\sqrt{f'_c} + 6900 \tag{5}$$

$$\left.\begin{matrix} f_{yh} \le 550MPa \\ f'_{co} > 75MPa \end{matrix}\right\} \rightarrow \beta = (0.048f'_{co} - 2.14) - \left(0.098f'_{co} - 4.57\right)\left(\frac{f'_l}{f'_{co}}\right)^{1/3} \tag{6}$$

$$\left.\begin{matrix} f_{yh} > 1200MPa \\ f'_{co} \le 80MPa \end{matrix}\right\} \rightarrow \beta = 0.07 \tag{7}$$

$$\left.\begin{matrix} f_{yh} > 1200MPa \\ f'_{co} > 80MPa \end{matrix}\right\} \rightarrow \beta = 0.1 \tag{8}$$

The regarding basic experimental data reported by Xiao and Yun, the initial calculated input values for HSC concrete are as **Table 2.** These values are used as preliminary data for evaluation of model and need further modifications. Based on the calculations, the input parameters for numerical model are also evaluated and reported in table.

3.3 Method and Simulation Procedure

The mathematical expression of governing response expressed in previous section is defined using OpenSees environment [16]. The nonlinear material response is integrated in internal integration point of elements and then is assembled in nodal regions considering geometrical nonlinearities. The member is modeled using three forced-based beam column elements that have conjugate nodes in lateral displacement applied level and stirrup spacing change location. Rebar and stirrup reinforcements characteristic is expressed STEEL02 uniaxial material code proposed by Menegoto and Pinto [17] with limitation in ultimate rupture strain (material failure) implied by MINMAX option. The elastic modules, initial yield strength and post-yield hardening ratio are 200 GPa, 473 MPa, and 0.5% respectively as reported in the original experimental data. However, the transition from the elastic to plastic branches is calibrated using 40, 0.925 and 0.15 for R_0, R_1, and R_2 coefficients respectively. It should be noted that higher R_0 values would lead to smoother transition in yielding threshold.

The physical model used for HSC material is assumed as CONCRETE01 proposed by Kent-Scott-Park [18], which is calibrated using compressive test data. However, calculated values are the preliminary data for analysis because HSC has lower ductility than NSC, which leads to calibration of degrading slope in detail. Due to lacking of material test data in Xiao and Yun research, the load-deflection curve of column is used for calibration of additional material parameters. The elastic modulus (E_c), unconfined (ε_{co}) and confined (ε_{cc}) crushing strain, confined axial strength (f'_{cc}), Descending Branch Slope Control (β) and lateral confining pressure (f'_l) are calculated based on the subsequent load-deflection curve shown in **Figure 4**. Figure shows the details of consecutive iterations made for primary calibration.

Geometric nonlinear response of column is to be modeled exactly as applied in experiment. For this purpose, the second-order axial force (P-Δ) effect is considered by means of axial load equal to 0.2 and 0.33 of nominal axial strength for FHC-1 and FHC-2 columns, respectively. Axial load is applied at the top elevation of column in numerical model and its time history is defined as constant over analysis domain. Integration of internal forces for column section is conducted by section fiber approach. Current method discretizes section into finite areas where strain is calculated according to defined uniaxial curve data and strain distribution along section domain. The patches for reinforcement and concrete volume are defined separately according to dimensional properties of test members. Generated element for HSC members is nonlinear beam-column with five integration points. Two types of data recorders for displacement in loading point (top) and base reaction (bottom) are generated. The load pattern of the lateral displacement is linear with respect to time and has cyclic regime. Calculation loop is defined for lateral load cycles, which has displacement control theory for integrator module and repeats three times for each drift ratio.

3.4 Simulation Results and Modification of Model

Based on the primary numerical results, cyclic response of FHC-1 and FHC-2 members are calculated as **Figure 5** and **Figure 6**. In order to compare the accuracy and validity of the developed model, the experimental data acquire by Xiao and Yun is plotted along with the results. Regarding figures, the post-peak softening of HSC members depends on post yielding slope of concrete material defined by β parameter. Due to lack of material test data in selected

experimental pilot, member response is analyzed with only change in β factor value and the stress-strain curve for each assumed value is generated. FHC-1 curve have conforming estimation for peak resisted base shear (V_f) equal to 683.60 kN and 2.7% lateral drift and these parameters for FHC-2 are 748.00 kN and 2% respectively. Current phenomenon shows that the stress-strain curve acquired by **Equation 1** and **Equation 2** gives identical results for HSC material. However, softening curve defined by **Equation 3** governs the backbone curve of members. Therefore, the ductility factor calculated for each assumed β factor needs to be analyzed and compared to existing experiment value.

Current study on the β value shows that the proposed relations as equation 6 up to 8 do not cover all the ranges of f'_c and f_y. This case is also mentioned in Bing et al. [7] research as the necessary investigation for β factor determination of HSC. The selected values for β factor cover the range between minimum (0.07) and maximum (0.25) for FHC-1 and the load curve for each case is extracted using numerical method, furthermore while minimum value for β is constant in FHC-2, maximum range changes to 0.22. Results show non-uniform variation of post peak softening with respect to β increase. Successive calculations proposed the β factor equal to 0.16 and 0.15 for FHC-1 and FHC-2 respectively. Within this assumption, acceptable accuracy achieved which provides 7.3% ultimate drift and 470 kN force level as reported in exactly in the experiment. According to various β, stress-strain curves that used in this research are as **Figure 7**. As the results show, within the increment in the β value, the concrete post-yield slope is increasing and this phenomenon controls the ductility of HSC. This observation is reported in **Table 3**. The study on the effect of β value on peak stress proved that it does not have sensible impact on the peak stress. However, the deformation ductility has close relation with the assumed β value.

4. Parametric Study

4.1 Axial Force Effect

One of the important parameters in assessment of energy dissipation is the axial force ratio. In order to estimate the energy-dissipation capacity of columns and its hysteretic behavior, variable axial force values are applied with respect to section nominal strength (P_n) that is estimated as 13950 kN in Xiao and Yun research. The relative value of these loads is beginning from 10% up to 50% of the section strength with $0.1P_n$ rise step. For the accurate and better evaluation of the column behavior, authors applied a collapse criterion based on the strength decay as 20% of ultimate shear force ($0.2V_n$). The extracted data curves are demonstrated in **Figure 8** with respect to the axial force increase. In the first step, the peak resisted base shear is 563 kN for 2% lateral drift in the column with $0.1P_n$ axial force and the column is also stable for further lateral drift values. The ultimate dissipated energy for this case is 1418 kN.m without any strength loss up to 8% drift.

Further increase in axial load up to $0.2P_n$ leads to 658 kN shear capacity of column at 2.4% lateral drift. Here, the axial load increases the load carrying capacity and ductility of HSC column by the simultaneous concrete crushing and rebar yielding. In this case, column starts to dissipate 1394 kN.m energy level with slight strength decrease due to the second-order axial force effect. In advance, further increase in axial force value up to $0.3P_n$ results in apparent decrease in energy dissipation of member to 840 kN.m and the ultimate drift to 6% although the shear strength is increased up to 720 kN. Additional increase of the axial force to $0.4P_n$ and $0.5P_n$ just lead in shear capacity to 760 kN and 790 kN respectively along with dissipated energy decrease to 480 kN.m and 470 kN.m, in that order. It is observed that axial load increase affects the energy dissipation capability of HSC members in a major manner and therefore such members are sensitive to the second-order effect. The drop ratios of absorbed energy value $0.3P_n$, $0.4P_n$ and $0.5P_n$ axial force

ratios are 40%, 60% and 70% consequently with respect to $0.1P_n$ case. In order to analyze the sensitivity of HSC columns to rebar ratio and axial force value, further numerical models are generated and are compared to the analogous case with NSC columns with 30 MPa concrete crushing strength in advance.

4.2 Rebar Ratio and Crushing Strength Effects

In order to have a better understanding of the effect of concrete strength on the hysteresis behavior, additional data with normal strength concrete is provided. NSC models obey the Mander et al. [15] proposed model for stress-strain curve as expressed in **Equation 9**. The longitudinal reinforcement ratio (ρ) is also considered as 1.3%, 2.6% and 3.9% values in order to consider the interaction of concrete and steel strengths in the calculation of the shear capacity and feasible energy dissipation. In addition, the axial force ratio is considered as $0.24P_n$ and $0.38P_n$ values in dimensionless form, not the same as the considered values in the previous section, to investigate the ductility sensitivity of HSC and NSC columns.

$$f'_{cc} = f'_{co}\left[-1.254+2.254\sqrt{1+7.94\frac{f'_l}{f'_{co}}}-2\frac{f'_l}{f'_{co}}\right] \tag{9}$$

The extracted data for assumed parameters are plotted in **Figure 9** for the shear strength history of HSC and NSC columns versus lateral cyclic drifts. Data are reported in **Table 4** considering various concrete strengths, rebar ratios and axial force ratio. For NSC and HSC columns with $0.24P_n$ axial force ratio (1600 kN and 3300 kN respectively), it was detected that the NSC column with the same rebar ratio as HSC member has better energy-dissipation than the HSC column. In addition, the pinching of HSC column hysteresis curve is increased which approves the lower energy dissipation of the member. Rebar ratios is 1.3%, 2.6%, and 3.9%. With study about the effect of rebar ratio, it was seen that rebar ratio is one of the significant parameters in HSCs. This result explain that we need to increase the maximum rebar ratio (ρ_{max}) of HSC members with respect to the limit which is defined for the normal strength elements. Since the high strength concrete has more brittle response than the normal strength concrete, we need further rebar ratio in order to provide the demand ductility in high strength concrete elements. Hence, in contrast to the idea, which the maximum rebar ratio is almost constant to the column elements, the designers of high strength members should extend the rebar ratio in order to provide the required energy dissipation during the earthquake excitation. Rebar ratio effect is shown in Figure 9 regarding hysteresis response and in **Figure 10** regarding the ultimate resisted shear force.

Ultimate shear strength (V_n), peak lateral drift (Δ) and total dissipated seismic energy (U_l) are plotted in **Figures 10** up to **12** respectively versus concrete grade (NSC and HSC), axial force ratio (P/P_n) and the rebar ratio (ρ). As shown in figure, the shear strength of column is increased when we change the concrete grade from NSC to HSC. In the next stage, within the raise of the axial force ratio, it was seen that the shear strength of column is increased. However, the effect of axial force ratio is more intuitive for the low rebar ratios, which means that within the increase in the axial force ratio for the low rebar amount, columns have better seismic performance and energy-dissipation. In the final stage, the shear strength of column is increased when we increase the rebar ratio. However, the HSC columns are more sensitive to the rebar ratio parameter than NSC one. In other words, HSC column need higher reinforcement ratio than NSC column in order to provide the required strength and the demand energy-dissipation.

We have plotted the variation of the peak lateral drift versus the aforementioned factors in **Figure 11**. In the first stage, it was seen that for a constant rebar ratio, the NSC column have better performance than HSC one. In addition, it was seen that the peak lateral drift in the HSC columns is decreasing when we increase the axial force ratio. However, this observation is in the reverse order for NSC columns. Finally, the increase in the rebar ratio results in the increase of the peak lateral drift in both of the concrete types. We have the maximum resisted lateral drift for 3.9% rebar ratio. In advance we investigated the dissipated energy level versus the aforementioned parameters in **Figure 12** for conclusion improvement. Primarily, it was seen that the energy absorbing is decreasing for concrete strength increase. However, this observation is not true for 3.9% rebar ratio. It means that we need to provide higher reinforcement ratio for HSC column to dissipate higher energy that NSC ones. The absorbed energy decreases while we increase the axial force level and this is more apparent in HSC columns the NSC ones. Analogous to the conclusion made for the peak lateral drift parameter, the absorbed energy is increase when we provide high rebar ratio. Overall conclusion is the requirement of higher rebar ratio for HSC column in order to provide better energy dissipation and ductility with respect to NSC columns.

5. Conclusions

Current research work deals with the seismic characteristics of the high strength concrete column subjected to lateral displacement cycles. We have provided the numerical models for initial validation of existing experimental results and then revised the governing stress-strain curve in order to improve the validity and accuracy of the developed nonlinear models. Results recommend that softening slope of the high strength concrete materials should be modified in order to approve the experimentally recorded ductility and energy-dissipation. In addition, we extended the models for normal strength and high strength concrete columns with variable axial force and reinforcement ratios in order to investigate the response sensitivity. The general conclusions made from the current research work can be mentioned as following topics.

1. The increase in the concrete grade and the axial force ratio results in shear strength enhancement of column. However, the peak lateral drift and the dissipated seismic energy is decreased. Therefore, it is required to provide higher reinforcement ratio than code-defined value in HSC to conform the response perquisite.
2. The Increase of rebar ratio results in improvement of ultimate shear strength, peak lateral drift, ductility and absorbed energy in HSC columns.
3. HSC columns can be appropriate choice for special structures only if the lateral drift and the absorbed energy is controlled by the existing code regulations.
4. Assuming analogous rebar ratio for HSC and NSC columns, NSC members can be more efficient than HSC in high-risk seismic zones.
5. Current study proposes a new modified concrete stress-strain curve considering linear interpolation between the β factors presented in previous research works for intermediate-strength HSC materials.

Abbreviation and Notation

Nomenclature	*description*
d	Rebar diameter
f_y	Yield stress
f'_{co} , f'_c	Unconfined Concrete compressive strength
P	Axial force
ε_{co}	Unconfined concrete strain
ε_{cc}	Confined concrete strain
E_c	Concrete modules of elasticity
β	Descending sloop control
f'_l	Lateral confining pressure
f'_{cc}	Confined concrete compressive strength
V_f	Peak resisted base shear
P_n	Section nominal strength
ρ_{max}	Maximum rebar ratio
V_n	Ultimate shear strength
ρ	Longitudinal reinforcement ratio
υ	Poisson ratio
Δ	Peak lateral drift
L	Elevation between lateral force point and foundation surface
R_0 , R_1 , R_2	Transition from elastic to plastic branch coefficient
U_I	Dissipated seismic energy

References

1. ACI Committee 363, "State-of-the-art Report on High-strength Concrete (ACI 363R-84)." *American Concrete Institute*, (1984).
2. Sugano, S., Nagashima, T., Kimura, H. and Tamura, H, "Experimental studies on seismic behavior of high strength concrete columns laterally reinforced with high strength steel bars." *Proceedings of the 9th WCEE*, Tokyo, Kyoto, (1988).
3. Xiao, Y. and Martirossyan, A., "Seismic performance of high-strength concrete columns." *Journal of Structural Engineering*, **124**(3), pp.241-251 (1998).
4. ASCE-ACI Task Committee 426, "The Shear Strength of Reinforced Concrete Members." *Journal of the Structural Division, Proceedings of the American Society of Civil Engineers (3rd)*, 99, pp.1091–1187 (1973).
5. ACI Committee 318, "Building Code Requirements for Structural Concrete (ACI 318M-02) and Commentary (ACI 318RM-02)" Metric Version. *American Concrete Institute*, (2002).
6. Ashour, S.A., "Effect of compressive strength and tensile reinforcement ratio on flexural behavior of high-strength concrete beams." *Engineering Structures*, **22**(5), pp.413-423, (2000).
7. Bing, L., Park, R. and Tanaka, H., "Stress-strain behavior of high-strength concrete confined by ultra-high-and normal-strength transverse reinforcements." *ACI Structural Journal*, **98**(3), pp.395-406 (2001).
8. Kabir, M.Z. and Shafei, E., "Plasticity modeling of FRP-confined circular reinforced concrete columns subjected to eccentric axial loading." *Composites Part B: Engineering*, **43**(8), pp.3497-3506 (2012).
9. Woods, J.M., Kiousis, P.D., Ehsani, M.R., Saadatmanesh, H. and Fritz, W., "Bending ductility of rectangular high strength concrete columns." *Engineering structures*, **29**(8), pp.1783-1790, (2007).
10. Ho, J.C.M., Lam, J.Y.K. and Kwan, A.K.H., "Effectiveness of adding confinement for ductility improvement of high-strength concrete columns." *Engineering Structures*, **32**(3), pp.714-725, (2010).
11. Lu, Z.H. and Zhao, Y.G., "Empirical stress-strain model for unconfined high-strength concrete under uniaxial compression." *Journal of Materials in Civil Engineering*, **22**(11), pp.1181-1186, (2010).
12. Ozbakkaloglu, T., "Behavior of square and rectangular ultra-high-strength concrete-filled FRP tubes under axial compression." *Composites Part B: Engineering*, **54**(1), pp.97-111, (2013).
13. Kottb, H.A., El-Shafey, N.F. and Torkey, A.A., "Behavior of high strength concrete columns under eccentric loads." *HBRC Journal*, **11**(1), pp.22-34, (2015).
14. Xiao, Y. and Yun, H.W., "Experimental studies on full-scale high-strength concrete columns." *ACI Structural Journal*, **99**(2), pp.199-207, (2002).
15. Mander, J.B., Priestley, M.J. and Park, R., "Theoretical stress-strain model for confined concrete." *ACI Journal of Structural Engineering*, **114**(8), pp.1804-1826, (1988).
16. OpenSees, "Open System for Earthquake Engineering Simulation." *Pacific Earthquake Engineering Research Center*, 2.4.6 (rev 6022), Copyright 1999-2013, The University of California, Berkley.
17. MENEGOTTO, M., "Method of analysis for cyclically loaded RC plane frames including changes in geometry and non-elastic behavior of elements under combined normal force and bending." *In Proc. of IABSE symposium on resistance and ultimate deformability of structures acted on by well-defined repeated loads*, pp. 15-22, (1973).
18. Scott, B.D., Park, R. and Priestley, M.J.N., "Stress-strain behavior of concrete confined by overlapping hoops at low and high strain rates." ACI journal, **79**(1), pp.13-27, (1982).

19. 

Farzin Vahid-Vahdattalab received the M.Sc. degree in structural engineering from the Urmia University of Technology, Urmia, Iran, in 2015. Present, he has been working on the high strength reinforced concrete columns under supervision of Dr. Erfan Shafei and Dr. Javad Mokari Rahmdel with focus on the nonlinear dynamic characteristics.

Dr. Javad Mokari Rahmdel received the Ph.D. degree in earthquake engineering from the International Institute of Earthquake Engineering and Seismology, Tehran, Iran, in 2009. Since then, he has been with Urmia University of Technology as Assistant Professor in civil engineering department, where he is currently the Administrative and Support.

Dr. Erfan Shafei (corresponding author) received the Ph.D. degree in structural engineering from the Amirkabir University of Technology (Tehran Polytechnic), Tehran, Iran, in 2013. Since then, he has been with the Urmia University of Technology as Assistant Professor in civil engineering department, where he is currently the Director of Civil Engineering Department. His research interest is on the nonlinear response assessment of semi-brittle materials.

Figures

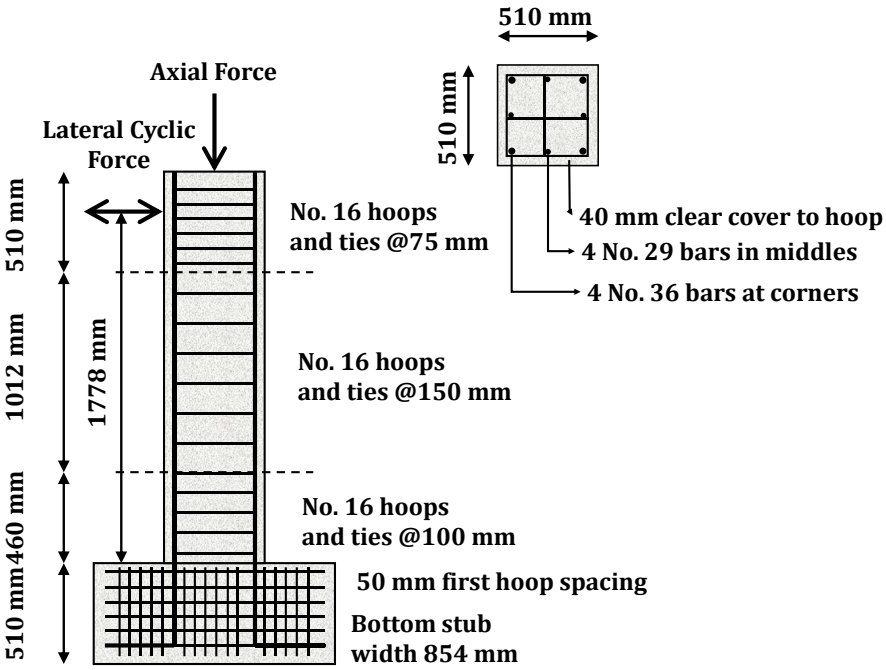

Figure 1: Detail of column specimens tested by Xiao and Yun [14]

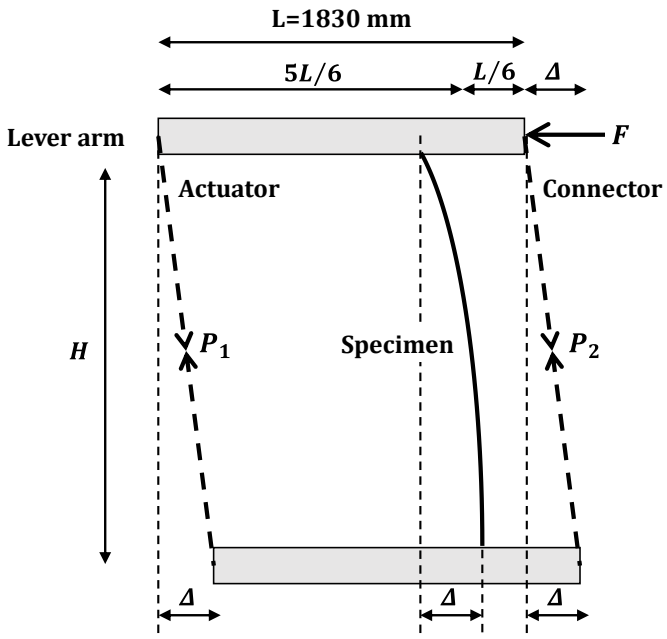

Figure 2: Lever arm system for axial loading and second order effect detail in test [14]

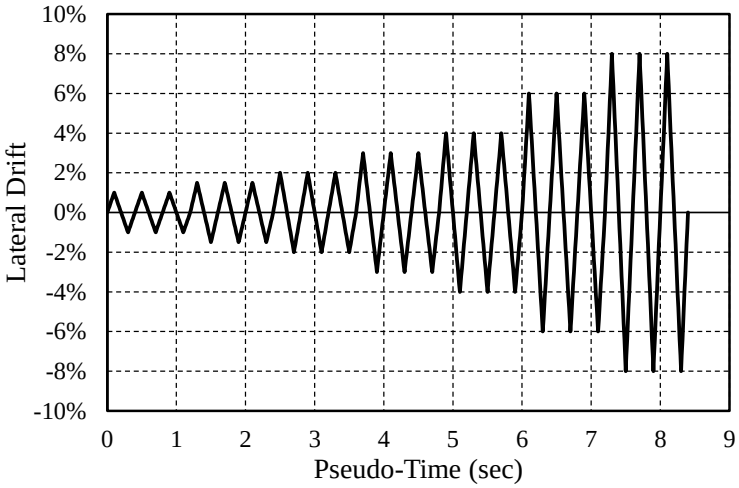

Figure 3: Time history curve of lateral drift applied to columns [14]

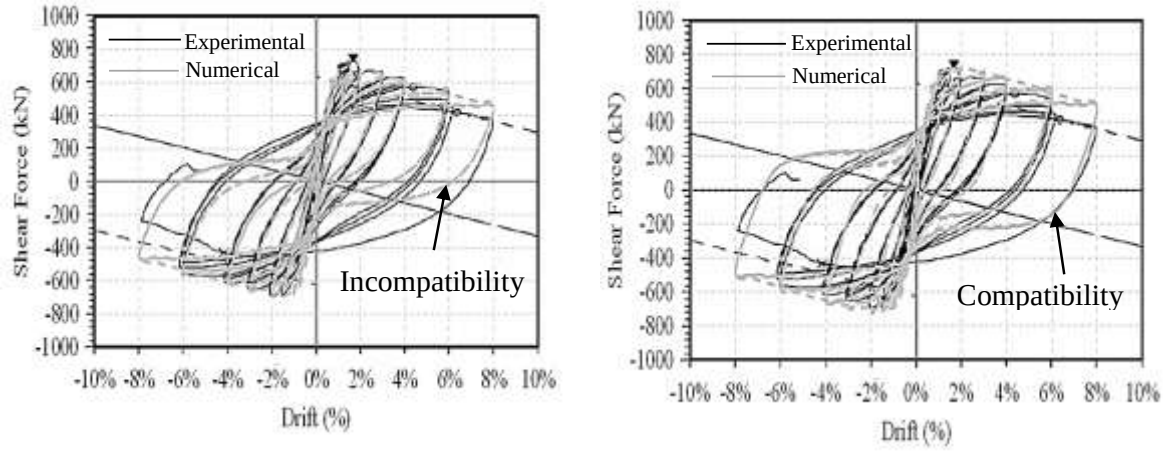

a: Before Calibration

b: After Calibration

Figure 4: Calibration Effect on Compatibility of Curves

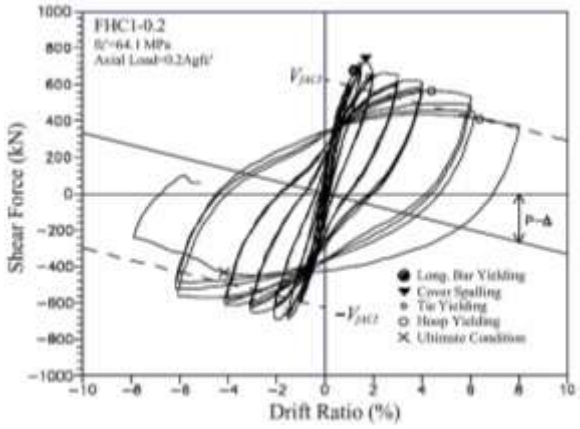

FHC-1 experiment result by Xiao and Yun [14]

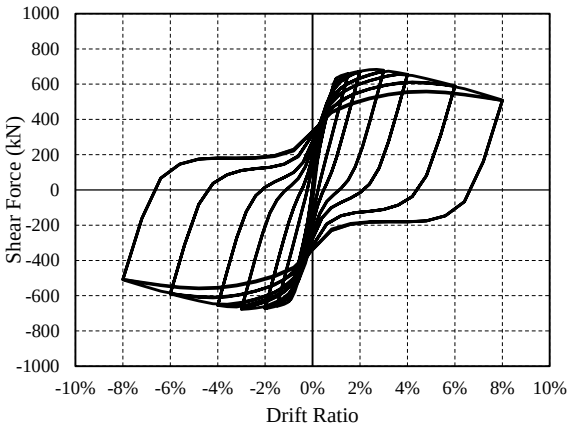

β=0.25 (Numerical Analysis)

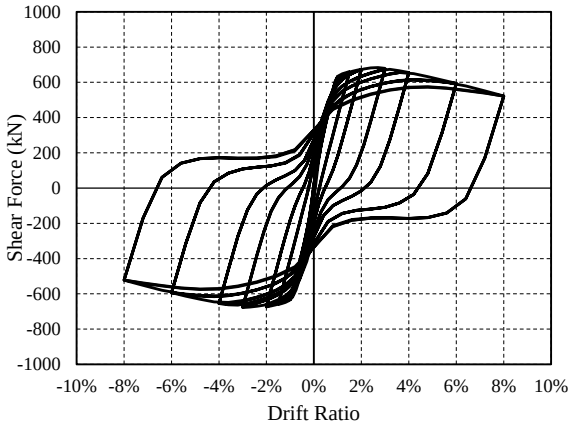

β=0.16 (Numerical Analysis)

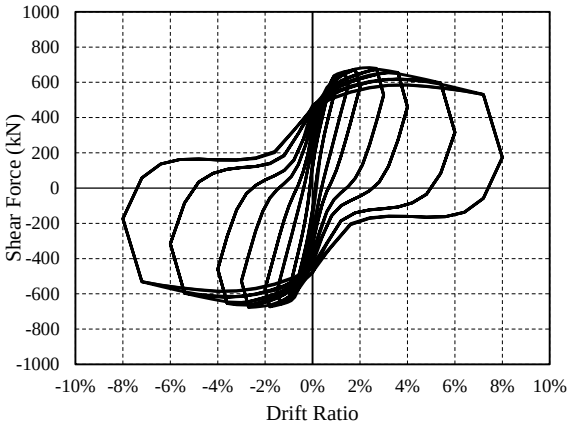

β=0.07 (Numerical Analysis)

Figure 5: Hysteresis load-displacement curves of FHC-1 column with various β factors

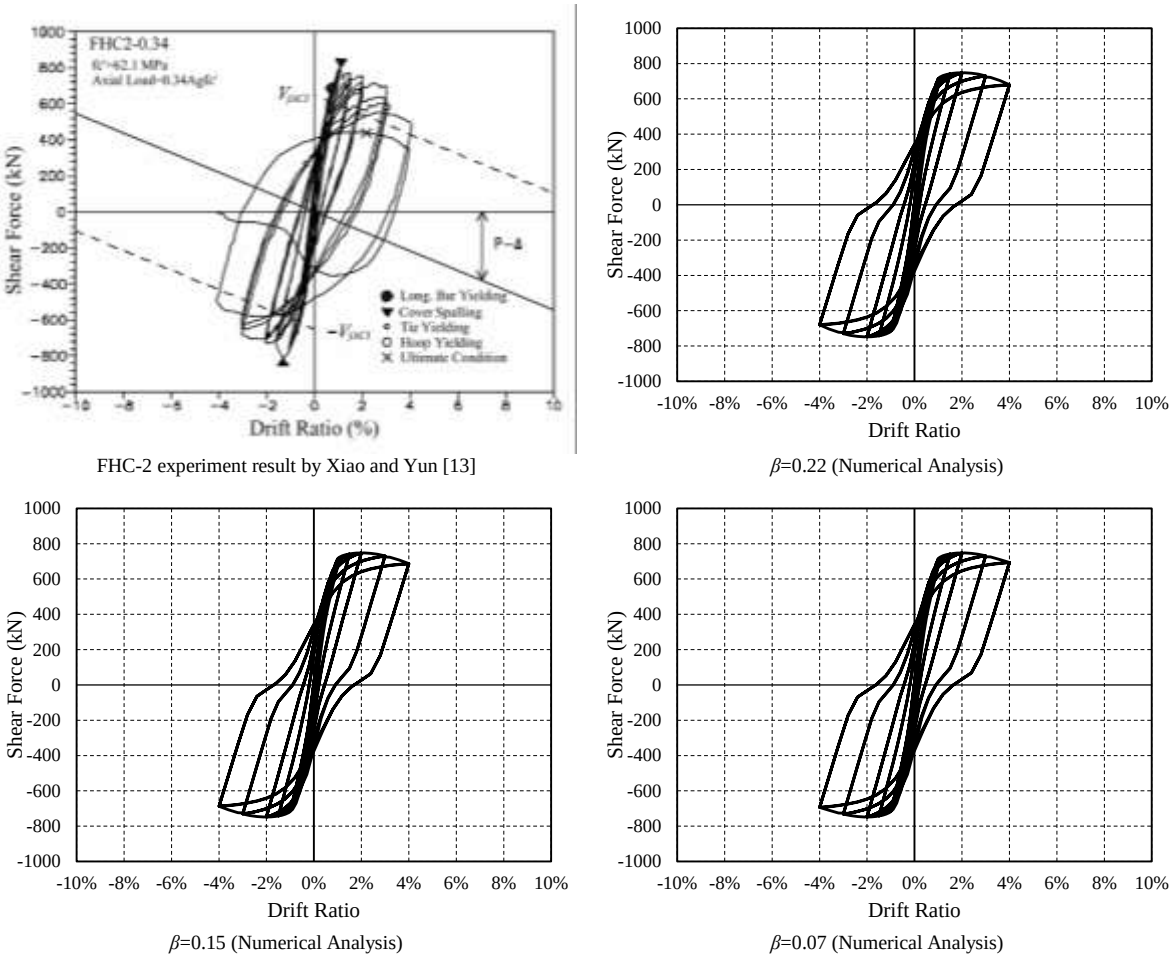

FHC-2 experiment result by Xiao and Yun [13]

β=0.22 (Numerical Analysis)

β=0.15 (Numerical Analysis)

β=0.07 (Numerical Analysis)

Figure 6: Hysteresis load-displacement curves of FHC-2 column with various β factors

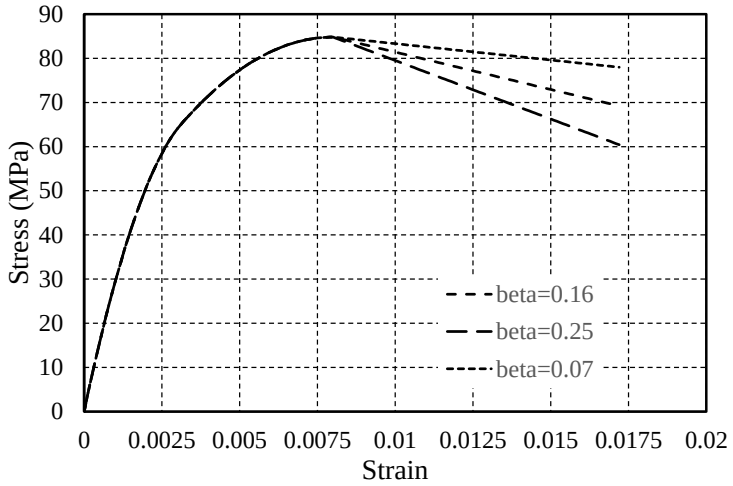

Figure 7: Envelope load-displacement curves for all columns with various β factors

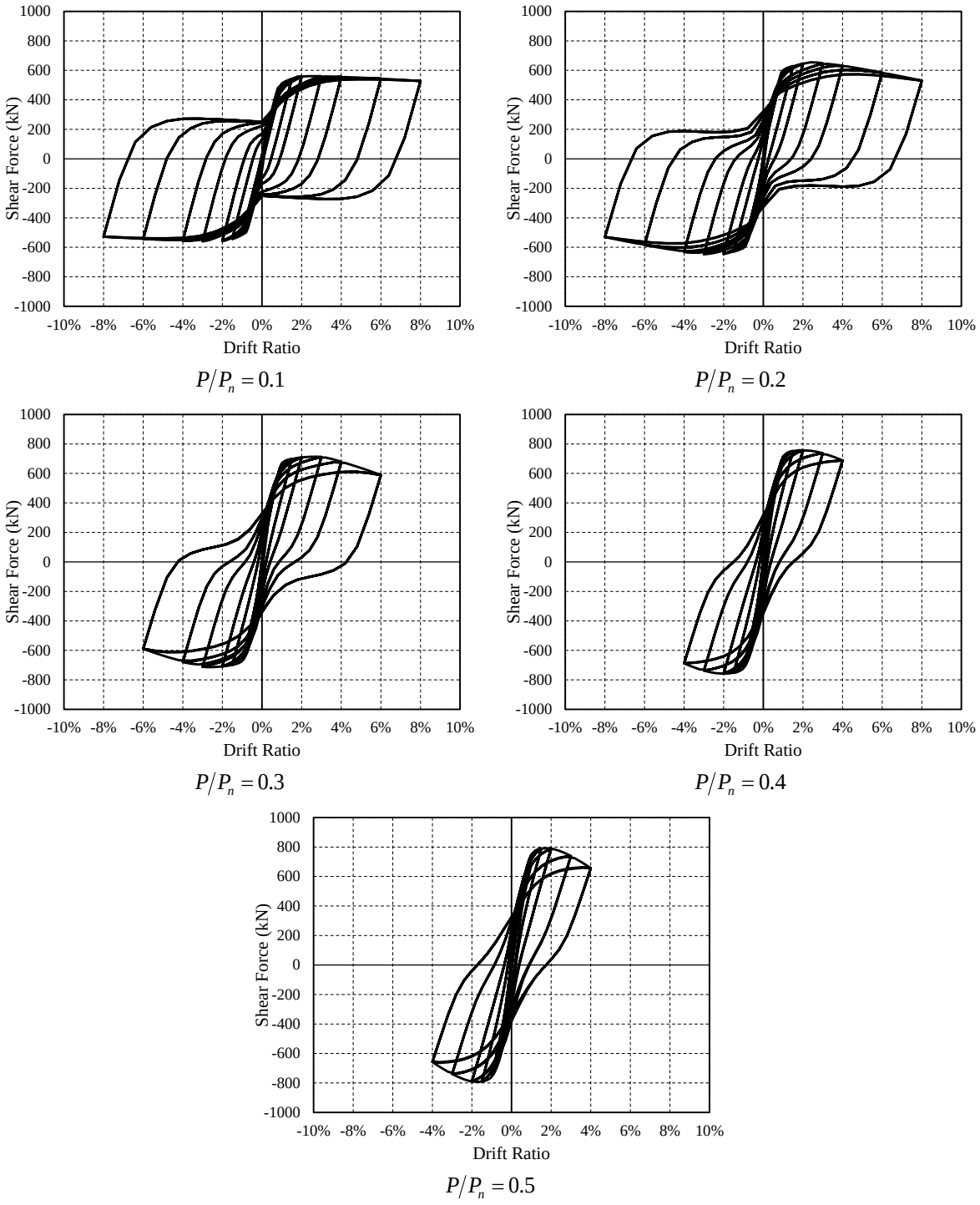

Figure 8: Axial load effect on hysteretic behavior of HSC columns (β=0.16)

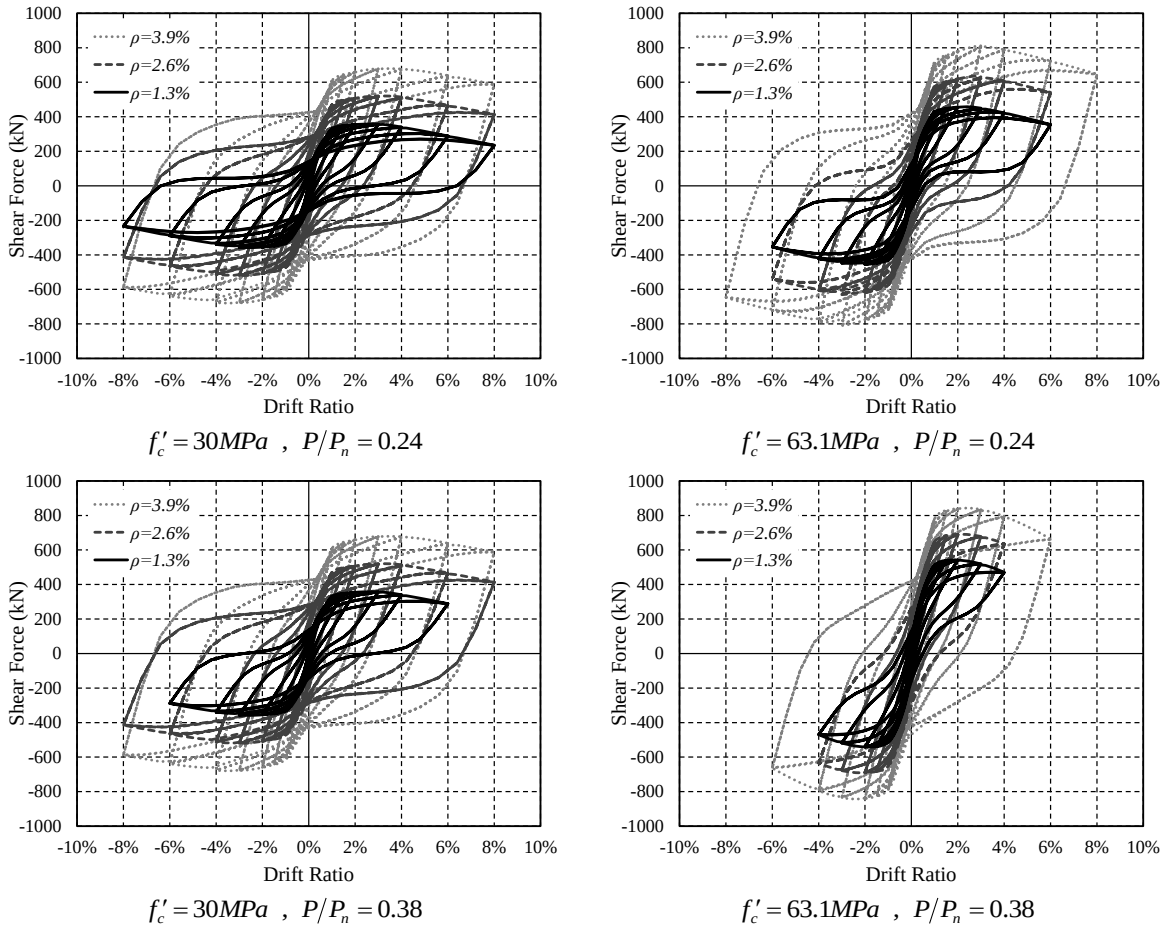

Figure 9: Shear Force versus lateral drift curves as function of concrete strength, axial load level and rebar ratio

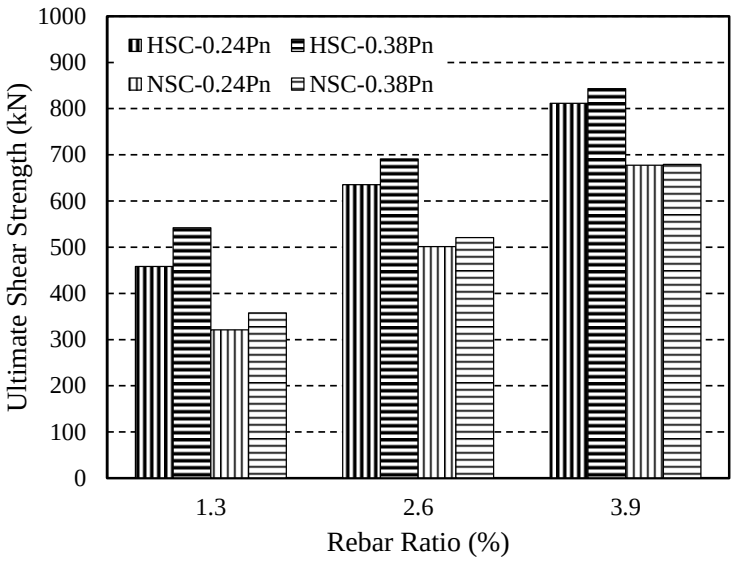

Figure 10: Shear strength of HSC and NSC columns with respect to axial load and rebar ratios

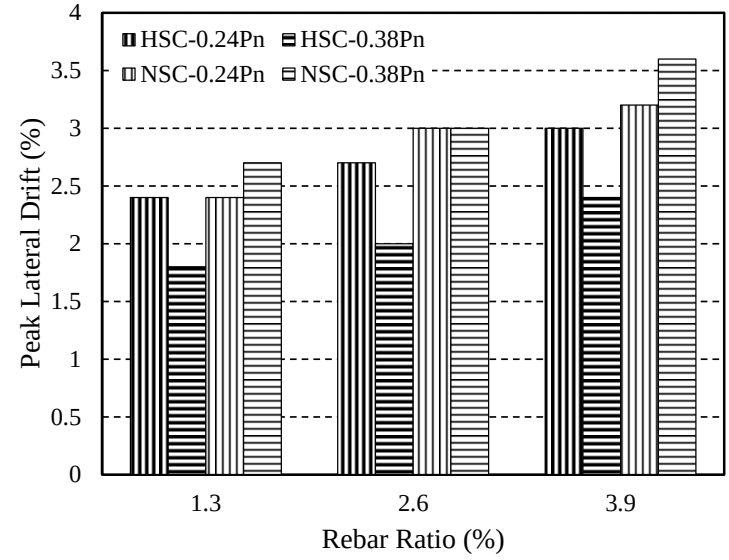

Figure 11: Peak lateral drift of HSC and NSC columns with respect to axial load and rebar ratios

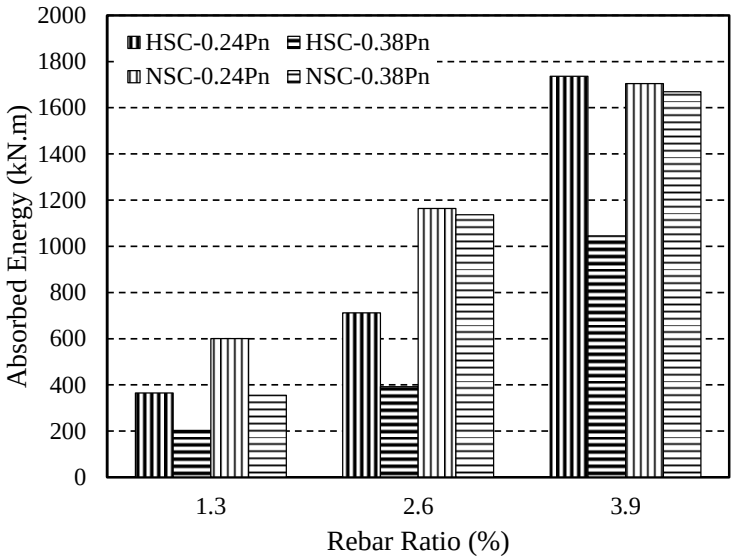

Figure 12: Absorbed seismic energy of HSC and NSC columns with respect to axial load and rebar ratios

Tables

Table 1: Details of HSC Column Members Tested by Xiao and Yun [13]

Specimens	Longitudinal Steel	Transverse Steel	Concrete Strength (MPa)	Axial Load (KN)
FHC-1	*4 Φ29 & 4Φ36*	Φ16 @100	64.1	3334
FHC-2		Φ16 @100	62.1	5373
FHC-3		Φ16 @100	62.1	3630
FHC-4		Φ16 @100	62.1	5240

Table 2: HSC Stress-Strain Curve Parameters and Input Values for Numerical Model

Parameter	Notation	Value		Unit
Elastic Modulus	E_C	33.481	33.063	GPa
Poisson's Ratio	υ	0.2		-
Unconfined Crushing Strain	ε_{co}	0.3		%
Confined Crushing Strain	ε_{cc}	0.8	0.8	%
Unconfined Crushing Stress	f'_{co}	64.1	62.1	MPa
Confined Crushing Stress	f'_{cc}	84.81	82.70	MPa
Descending Branch Slope Control	β	0.16	0.15	-
Lateral Confining Pressure	f'_l	4.19	4.19	MPa
OpenSees – Crushing Stress	fpc	84.81	82.70	MPa
OpenSees – Crushing Strain	epsc0	0.8	0.8	%
OpenSees – Failure Stress	fpcu	33.92	33.08	%
OpenSees – Failure Strain	epsu	3.8	4	%

Table 3: Effect of β value on ultimate ductility

Specimens	*Procedure*	β	Δ_u/Δ_y
FHC-1	Numerical	0.16	2.67
	Experimental	-	2.44
FHC-2	Numerical	0.16	2.0
	Experimental	-	2.1

Table 4: Calculated response parameters of NSC and HSC column members

Specimens	*Axial Force Ratio*	*Rebar Ratio*	*Shear Capacity*	*Peak Drift*	*Dissipated Energy*
Unit	-	*%*	*kN*	*%*	*kN.m*
HSC-1	0.24	1.3	458.4	2.4	365.2
HSC-2	0.24	2.6	635.4	2.7	711.9
HSC-3	0.24	3.9	811.5	3.0	1736.4
HSC-4	0.38	1.3	542.0	1.8	202.6
HSC-5	0.38	2.6	691.0	2.0	391.8
HSC-6	0.38	3.9	843.1	2.4	1045.0
NSC-1	0.24	1.3	321.2	2.4	600.2
NSC-2	0.24	2.6	501.1	3.0	1164.2
NSC-3	0.24	3.9	677.4	3.2	1704.6
NSC-4	0.38	1.3	357.7	2.7	355.33
NSC-5	0.38	2.6	520.6	3.0	1136.6
NSC-6	0.38	3.9	679.3	3.6	1669.2